JCTC Journal of Chemical Theory and Computation

Article

pubs.acs.org/JCTC

Collective Reaction Coordinate for Hybrid Quantum and Molecular Mechanics Simulations: A Case Study of the Hydride Transfer in Dihydrofolate Reductase

Dvir Doron,[†] Amnon Kohen,[‡] and Dan Thomas Major*[,†]

[†]Department of Chemistry and the Lise Meitner-Minerva Center of Computational Quantum Chemistry, Bar-Ilan University, Ramat-Gan 52900, Israel

[‡]Department of Chemistry, University of Iowa, Iowa City, Iowa 52242, United States

Supporting Information

ABSTRACT: The optimal description of the reaction coordinate in chemical systems is of great importance in simulating condensed phase reactions. In the current work, we present a collective reaction coordinate which is composed of several geometric coordinates which represent structural progress during the course of a hydride transfer reaction: the antisymmetric reactive stretch coordinate, the donor−acceptor distance (DAD) coordinate, and an orbital rehybridization coordinate. In this approach, the former coordinate serves as a distinguished reaction coordinate, while the latter two serve as environmental, Marcus-type inner-sphere reorganization coordinates. The classical free energy surface is obtained from multidimensional quantum mechanics−molecular mechanics (QM/MM) potential of mean force (PMF) simulations in conjunction with a general and efficient multidimensional weighted histogram method implementation. The minimum free energy path, or the collective reaction coordinate, connecting the dividing hypersurface to reactants and products, is obtained using an iterative scheme. In this approach, the string method is used to find the minimum free energy path. This path guides the multidimensional sampling, while the path is adaptively refined until convergence is achieved. As a model system, we choose the hydride transfer reaction in *Escherichia coli* dihydrofolate reductase (*ec*DHFR) using a recently developed accurate semiempirical potential energy surface. To estimate the advantages of the collective reaction coordinate, we perform activated dynamics simulations to obtain the reaction transmission coefficient. The results show that the combination of a distinguished reaction coordinate and an inner-sphere reorganization coordinate considerably reduces the dividing surface recrossing.

1. INTRODUCTION

Transition state theory (TST) forms a fundamental theoretical framework for studying chemical kinetics.[1] The basic and generalized[2] forms of TST were initially developed for gas-phase reactions but have been extended to treat reactions in solutions[3] and in enzymes.[4−6] In generalized TST, the rate constant may be defined as

$$k = \frac{1}{2}\gamma\cdot\langle|\dot{\zeta}|\rangle\cdot\frac{\rho(\zeta^{\ddagger})}{\int_{\zeta_{RS}}\rho(\zeta)\,\mathrm{d}\zeta} \tag{1}$$

where $\rho(\zeta)$ is the probability density at a given position along a reaction coordinate, ζ.[7] In particular, $\zeta^{\ddagger}$ is the value of the reaction coordinate at the transition state (TS), i.e., the hypersurface dividing the reactant state (RS) and the product state (PS) regions. $\langle|\dot{\zeta}|\rangle$ is the average absolute value of the crossing velocity, $\dot{\zeta} = d\zeta/dt$, evaluated at $\zeta^{\ddagger}$.[8] γ is a composite transmission coefficient accounting for dynamical recrossing at the TS (κ), quantum mechanical tunneling, and nonequilibrium effects.[9,10] The potential of mean force (PMF) is defined by

$$W(\zeta) = -\frac{1}{\beta}\ln\rho(\zeta) + C \tag{2}$$

where $\beta = (k_B T)^{-1}$, k_B is Boltzmann's constant, T is the temperature, and C is an undetermined constant. The PMF may be computed from molecular dynamics (MD) simulations in conjunction with umbrella sampling (US).[11,12] The dynamical recrossing transmission coefficient may be obtained from the following expression:[13,14]

$$\kappa(t) = \frac{\langle\dot{\zeta}(0)\,\theta[\zeta(t) - \zeta^{\ddagger}]\rangle_{\zeta^{\ddagger}}}{\langle\dot{\zeta}(0)\,\theta[\dot{\zeta}(0)]\rangle_{\zeta^{\ddagger}}} \tag{3a}$$

where the brackets in the numerator and the denominator, $\langle(...)\rangle_{\zeta^{\ddagger}}$, denote an ensemble average over TS configurations, $\dot{\zeta}(0)$ is the velocity of the reaction coordinate at time zero, and $\theta(x)$ is the Heaviside step function taking a value of 1 when x is positive and 0 otherwise. Specifically, $\theta(x) = 1$ for values of reaction coordinate at time t, which correspond to the PS well (i.e., $\zeta(t) > \zeta^{\ddagger}$), or for initially positive velocities heading toward the PS well (i.e., $\dot{\zeta}(0) > 0$). More practically, it can be shown that by separating the initial velocities into positive and negative contributions, and inserting $\theta[\dot{\zeta}(0)] + \theta[-\dot{\zeta}(0)] = 1$ into the numerator of eq 3a, the time-dependent transmission coefficient may be expressed as[14,15]

Received: March 22, 2012
Published: June 25, 2012

   dx.doi.org/10.1021/ct300235k | J. Chem. Theory Comput. 2012, 8, 2484−2496

$$\kappa(t) = \frac{\langle \dot{\zeta}(0)\, \theta[\dot{\zeta}(0)]\, \theta[\zeta(t) - \zeta^{\ddagger}] \rangle_{\zeta^{\ddagger}}}{\langle \dot{\zeta}(0)\, \theta[\dot{\zeta}(0)] \rangle_{\zeta^{\ddagger}}} - \frac{\langle \dot{\zeta}(0)\, \theta[-\dot{\zeta}(0)]\, \theta[\zeta(t) - \zeta^{\ddagger}] \rangle_{\zeta^{\ddagger}}}{\langle \dot{\zeta}(0)\, \theta[-\dot{\zeta}(0)] \rangle_{\zeta^{\ddagger}}}$$

$$= \langle \theta[\zeta(t) - \zeta^{\ddagger}] \rangle_{+} - \langle \theta[\zeta(t) - \zeta^{\ddagger}] \rangle_{-} \quad (3b)$$

where

$$\langle (\cdots) \rangle_{\pm} = \frac{\langle \dot{\zeta}(0)\, \theta[\pm\dot{\zeta}(0)](\cdots) \rangle_{\zeta^{\ddagger}}}{\langle \dot{\zeta}(0)\, \theta[\pm\dot{\zeta}(0)] \rangle_{\zeta^{\ddagger}}} \quad (3c)$$

represents an average over fractional equilibrium distributions distinguished by either positive or negative initial velocities. The transmission coefficient, κ, is obtained by the initial plateau value of the function $\kappa(t)$.

The computation of the PMF as well as the transmission coefficient depends on the choice of the reaction coordinate, ζ. Indeed, the reaction coordinate is an essential tool to quantify the progress of chemical transformations in the gas phase and in condensed phases and may give considerable insight into the nature of the transitions state. However, it is not obvious how to choose the reaction coordinate, in particular in complex condensed phase environments. In simulations of systems crossing a considerable barrier, it is necessary to apply some form of a biasing potential to the reaction coordinate (e.g., US), and the sampling efficiency may depend on the reaction coordinate definition.

In reactions where little is known about the details of the path, various approaches have been devised which search for the optimal reaction coordinate. Such approaches include reaction path search methods,[16] transition path sampling,[17,18] and the nudged elastic band algorithm.[19,20] One may also combine US with path finding methods, to achieve an enhanced description of the reaction coordinate in condensed phases such as enzymes.[21−23] Typically, the path-based approaches result in collective reaction coordinates that include contributions from a multitude of coordinates.

The reaction coordinate may be defined as a geometric function, such as bond distances and angles, that change during the conversion of a RS to a PS.[24−27] This approach is frequently used in conjunction with molecular orbital (MO) and density functional theory (DFT) approaches to condensed phase reactions. In this approach, it is implicitly assumed that degrees of freedom orthogonal to the reaction coordinate relax in response to changes in the reaction coordinate along the reaction path. Alternatively, the reaction coordinate may be defined as a collective bath coordinate, as in Marcus theory.[28−33] This collective bath coordinate is defined as the energy difference between two diabatic states.[34] The energy gap coordinate allows the multidimensional solvent effect to be described by a single variable which corresponds to the changing of the solute along the reaction coordinate in a fixed solvent ensemble.[35] This approach has been used in valence bond (VB) methods, such as empirical valence bond (EVB) simulations,[30,31] hybrid MOVB approaches,[32,33] and pure VB approaches.[36,37] Geometric coordinates and energy gap coordinates have been compared and found to yield similar dynamical recrossing transmission coefficient for selected systems.[24] Combined approaches employing both geometric and energy gap coordinates have also been used.[38]

The advantage of collective reaction coordinates or energy gap coordinates is that they naturally include environmental effects, thus assuring that the environment is properly relaxed along the reaction coordinate. Additionally, such coordinates may result in reduced recrossing of the dividing surface and have been employed, in addition to simple chemical coordinates, in previous work.[38,39] However, collective reaction coordinates are not chemically intuitive coordinates. Haddon and Chow introduced hybridization as an alternative general metric for reaction progress and as a universal reaction coordinate in various reactions in the gas-phase.[40,41] Rehybridization is an attractive reaction coordinate as it presents a metric which is intuitive for most chemists. It would thus be useful to employ rehybridization as a reaction coordinate in complex environments. Previously, the hybridization states have been analyzed from MD trajectories of enzymatic reactions.[42−44] Pu et al. presented a nonlinear relationship between reaction progress and hybridization states, showing the benefits in using the hybridization state as a complementary measure of reaction progress.[42] Asynchronous progress of rehybridization was also found for alcohol dehydrogenase by Roston and Kohen.[18]

In the current work, we derive a unified reaction coordinate based on three geometric coordinates: antisymmetric stretch reaction coordinate, donor−acceptor distance, and the rehybridization difference between the donor and acceptor atoms. The latter two reaction coordinates are independent of the coordinates of the transferring atom and may be considered as describing inner-sphere reorganization as in Marcus theory.[28,46] Multidimensional US simulations are performed in combination with an efficient multidimensional implementation of the weighted histogram analysis method (WHAM).[47] These three reaction coordinates were integrated to a collective reaction coordinate (CRC) based on the minimum free energy path (MFEP) obtained using the string method.[48−50] This approach is used to study the hydride transfer in *Escherichia coli* dihydrofolate reductase (*ec*DHFR) using a recently developed hybrid quantum mechanics (QM)−molecular mechanics (MM) potential energy surface.[51] The hydride transfer in DHFR (Scheme 1) has been studied by numerous researchers both experimentally[52−59] and computationally[42,51,60−68] and serves as an important benchmark system in enzymology.

2. METHODOLOGY

Model of the Enzyme−Substrate−Coenzyme Complex. The initial coordinates used to build the model for the present study were based on the crystal structure of a complex of *ec*DHFR with folate, $NADP^+$, and water molecules (PDB ID

Scheme 1. The Hydride Transfer Reaction Catalyzed by DHFR[a]

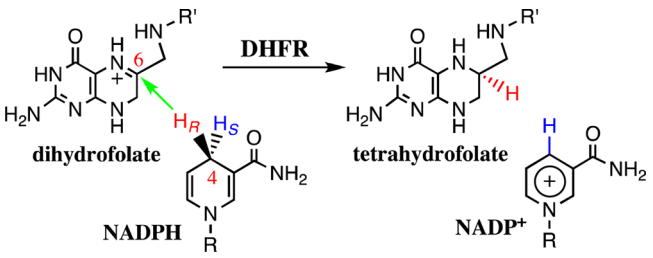

[a]R: adenine dinucleotide 2′-phosphate. R′: *p*-aminobenzoyl-glutamate.

code 1RX2[69]), where the Met20 loop is in the closed conformation. The original ligands in this structure were exchanged by N5-protonated 7,8-dihydrofolate and NADPH, to form a model of the reactive Michaelis complex. Out of the 159 amino acid residues, all ionizable residues were treated as bearing protonation states that match neutral pH.[52−54] In particular, Asp27 was modeled as deprotonated,[70−72] and the specific protonation states of the histidine residues were determined on the basis of hydrogen bonding interactions. This model was soaked in a pre-equilibrated 65 × 65 × 65 Å^3 cubic water box and thereafter neutralized by adding 14 sodium ions to allow evaluation of electrostatic interactions using the Ewald summation scheme. The final model is comprised of 27 986 atoms. Further details have been provided elsewhere.[51]

Potential Energy Surface. The potential energy surface (PES) in the current study is described by a hybrid QM/MM Hamiltonian.[73−75] The QM region consists of 69 atoms, including portions of the substrate and coenzyme that are in proximity to the reaction center, along with two link atoms. This part is described by a modified AM1 semiempirical Hamiltonian,[76] where the parameters have been optimized to treat model reactions involving various derivatives of nicotinamide and pterin compounds (specific reaction parameters, denoted AM1-SRP).[51] The MM part contains the protein, water, ions, and the remaining substrate and coenzyme atoms not described by QM. The MM atoms are treated by the CHARMM22/27 force field[77,78] with grid-based energy correction maps (CMAP)[79] for peptide dihedral angles, and water molecules are represented by the three-point charge TIP3P model.[80] QM/MM interactions are treated by electrostatic embedding wherein the MM partial atomic charges are included in the one-electron Hamiltonian. QM/MM interaction energies between the reacting fragments (QM) and the protein (MM) were fine-tuned by modifying the van der Waals parameters of the QM hydrogen atoms.[81] This combined potential energy was shown to yield accuracy comparable to density functional theory (DFT), giving accurate results for the hydride transfer reaction in *ec*DHFR.[51] All simulations employed the CHARMM program.[82,83]

Molecular Dynamics Simulations. Periodic boundary conditions (PBC) were applied, and the Ewald method was employed for reciprocal space summations between MM sites as well as for the QM/MM interactions (64 × 64 × 64 FFT grid, κ = 0.340 Å^{-1}).[84] A 13.0 Å group-based cutoff was applied for van der Waals and electrostatic interactions. All atoms were gradually relaxed at the MM level of theory to remove close contacts in the initial protein−ligand−solvent model. The isothermal−isobaric (NPT) ensemble was employed at 298 K and 1 atm using the extended pressure/temperature (CPT) algorithm[85,86] with a Hoover thermostat.[87] The leapfrog integration scheme[88] was used to propagate the equations of motion, and the SHAKE algorithm[89] was applied to constrain all MM bonds involving hydrogen atoms, allowing a time step of 1 fs. The system was heated up in a stepwise fashion from 48 to 298 K for 25 ps and thereafter equilibrated at the target temperature (298 K) over the course of 1 ns at the MM level of theory, with further 200 ps of equilibration using the QM(AM1-SRP)/MM potential. Further details of the MD simulations are available in ref 51.

Free Energy Simulations. The classical mechanical PMF (CM-PMF) associated with the *ec*DHFR-catalyzed hydride transfer reaction was obtained by employing adaptive US MD simulations, combined with a multidimensional implementation of WHAM.[11] In this study, we defined three types of reaction coordinates, representing different measures of progress with respect to the hydride transfer reaction.

The first reaction coordinate is the traditional antisymmetric stretch coordinate, which is the difference between the donor carbon−hydrogen bond (C4N−H) and acceptor carbon−hydrogen bond (C6−H) distances, that is

$$\zeta_{\mathrm{asym}} = R(\mathrm{C4N{-}H}) - R(\mathrm{C6{-}H}) \tag{4}$$

This type of reaction coordinate has been employed extensively in the literature in QM/MM free energy simulations of enzymatic reactions,[90] in particular H-atom transfer reactions[24] including DHFR catalysis.[42,51,61,91] The antisymmetric stretch reaction coordinate has been shown to give similar energetic results to energy gap coordinates.[61] In our introductory work,[51] we employed the QM(AM1-SRP)/MM Hamiltonian as a potential energy surface for US simulations that were guided by imposing a biasing potential on the antisymmetric stretch coordinate, thereby determining the one-dimensional PMF. This basic approach of sampling the reaction free energy will henceforth be termed "1D$_{\mathrm{asym}}$".

The second reaction coordinate considered in the current study is the donor−acceptor distance (DAD)

$$\zeta_{\mathrm{DAD}} = R(\mathrm{C4N{-}C6}) \tag{5}$$

For the DHFR catalyzed reaction, the DAD was shown in several works[58−60,92,93] to play a prominent role in enzyme catalysis as a varying property which correlates with the progress of the hydride transfer and was found to be compressed to the shortest distance near the transition state. Hammes-Schiffer and co-workers have identified the DAD fluctuations as part of a "network of coupled promoting motions",[92] namely systematic changes of thermally averaged geometrical properties that occur as the reaction evolves from the reactant to the transition state. Interestingly, Miller and co-workers found the DAD to be strongly correlated with the dynamics of the hydride transfer.[67] In examination of the effect of remote mutants on the DHFR reaction, Liu and Warshel specifically presented the PMF as a function of the DAD and found the DAD to be dependent on mutant and temperature.[66] We have recently computed the momentum distribution at selected DADs using open-chain path integral simulations in order to assess the correlation between quantum delocalization of the transferring hydride at the TS and the DAD.[68]

Finally, the third reaction coordinate describes the difference between the hybridization states, χ, of the hydride acceptor (C6) and hydride donor (C4N) carbon atoms

$$\zeta_{\mathrm{rehyb}} = \chi(\mathrm{C6}) - \chi(\mathrm{C4N}) \tag{6}$$

As this quantity expresses the relative hybridization, we shall refer to the definition in eq 6 as the rehybridization coordinate. The evaluation of the two hybridization states relies on the model formulated by Pu et al.[42] Briefly, this model exploits the instantaneous local geometry of the DAD carbon atoms and their corresponding substituents during MD simulations. For each center, three "auxiliary" sp$^{\chi}$ hybrid orbitals are defined along the bonds of the neighboring nontransferring atoms, where χ is the hybridization state variable measuring the extent of the p contributions to each hybrid orbital.[42] This variable can be represented as the squared ratio of the coefficients of s and p components of the auxiliary orbitals, where the latter is expressed in terms of the "active" hybrid orbital involved in the

σ-bonding with the transferring hydride. It follows that the hybridization state can be linearly correlated with L, the distance from the central carbon atom to the plane, determined by the positions of its three substituents (excluding the position of the transferring hydride), in the form

$$\chi = 2 + 3L \tag{7}$$

Taking advantage of this definition, we note that substitution of eq 7 into eq 6 yields

$$\zeta_{\mathrm{rehyb}} = 3\cdot(L_{\mathrm{acceptor}} - L_{\mathrm{donor}}) \tag{8}$$

which is the actual form used for all calculations mentioned in this study involving the rehybridization coordinate. The order of subtraction of the terms was intentionally chosen so as to be consistent with the sign of the antisymmetric stretch coordinate in the reactant and product states. In addition, the boundary conditions for ζ_{rehyb} can be generally determined by association of *ideal* initial and final hybridization states with the acceptor and donor carbons.[40] More specifically, in the RS of the DHFR catalyzed reaction, the C6 (hydride acceptor) and C4N (hydride donor) carbons adopt approximate sp^2 and sp^3 hybridizations, respectively, which correspond to $\chi(\mathrm{C6}) = 2$ and $L_{\mathrm{acceptor}} = 0$ Å and to $\chi(\mathrm{C4N}) = 3$ and $L_{\mathrm{donor}} = 1/3$ Å. Accordingly, the bottom boundary of ζ_{rehyb} will be given a theoretical value of −1 Å; whereas the PS is characterized by swapped hybridization states with tetrahedral symmetry of C6 and trigonal planar geometry of C4N, i.e., $\chi(\mathrm{C6}) = 3$ and $L_{\mathrm{acceptor}} = 1/3$ Å and $\chi(\mathrm{C4N}) = 2$ and $L_{\mathrm{donor}} = 0$ Å, resulting in an upper limit value of 1 Å. It should be noted though that in practice, this theoretical scale might exceed the idealized limits mainly due to two reasons: First, the hybridization is ultimately expressed in this reaction coordinate by means of geometrical quantities, and not by explicit electronic terms (note the use of distance units, Å, rather than keeping the rehybridization coordinate dimensionless). Second, for simplification purposes, the model assumes equal distributions of s and p components among all three "auxiliary" sp^{χ} hybrid orbitals.[42]

To assess the extent to which the three types of reaction coordinates facilitate hydride transfer, three schemes of simulations were carried out, distinguished by the choice of the subset of reaction coordinates employed and subjected to biasing potential during US MD simulations. In each scheme, coordinates with no biasing force applied were used as spectator coordinates, and their instantaneous values are employed to keep track of the configurations sampled along with the restrained coordinate. Clearly, the addition of spectator coordinates is not to enhance sampling but rather to ensure that the reaction proceeds through a narrower reactive funnel. A more precise description of the dividing surface is expected to result in reduced recrossing (*vide infra*).

In the first scheme,[51] a series of 13 discrete regions ("windows") along the antisymmetric stretch reaction coordinate was defined with uniform spacing of 0.25 Å, while a harmonic restraint was centered at each of them. The harmonic force constants, k, ranged between 20.0 and 60.0 kcal·mol^{-1}·Å^{-2} [$E_{\mathrm{harm}} = k(\zeta - \zeta_{\mathrm{ref}})^2$]. The antisymmetric coordinate was also subject to an umbrella potential, which is basically the negative of the PMF obtained in the preceding series of simulations. The probability distribution was collected along the antisymmetric stretch coordinate only. We shall label this restraining scheme in this paper as "1D$_{\mathrm{asym}}$".

In the second scheme, 16 "windows" were used to span the entire range of the antisymmetric stretch coordinate in a similar fashion to that employed in the "1D$_{\mathrm{asym}}$" scheme. In these simulations, the DAD and rehybridization coordinates were used as spectator coordinates. This restraining scheme will be referred to henceforth as "3D$_{\mathrm{asym}}$".

In the third scheme, termed "3D$_{\mathrm{DAD/rehyb}}$", the two other reaction coordinates were biased, namely, the DAD and the rehybridization coordinates. These were both restrained using harmonic force constants (25.0−70.0 kcal·mol^{-1}·Å^{-2}), and an umbrella potential was additionally applied to the DAD coordinate. This combination of the DAD and rehybridization coordinates attempts to describe the hydride transfer *indirectly* without involving explicitly the position of the H atom.

We note that the latter two schemes present the reaction coordinate as a combination of a distinguished chemical reaction coordinate and a solvent-like coordinate.[45]

Specifically, after the initial guess free-energy surface was constructed for the multidimensional PMF simulations, the string method (*vide infra*) was employed to find the optimal path connecting the reactant and product states on this multidimensional surface. Subsequently, an updated umbrella sampling series was run along this path (now consisting of new discrete values of the reaction coordinates), resulting in an updated surface. In turn, the latter was used to calculate a new optimal string and so forth. In practice, we took advantage of a new multidimensional implementation of WHAM (see below) to produce multidimensional free energy surfaces. Additionally, we derived free energy iso-surfaces, i.e., "slices", of the complete multidimensional free energy surface along a chosen reaction coordinate to ensure adequate and continuous sampling. This combined approach was continued until the MFEP was converged.

In both 3D sampling schemes, each US window was sampled in 5−6 series. Each series was equilibrated for 2 ps, followed by 100 ps of production simulation that collected the probability densities of configurations (ρ) along the reaction coordinates and sorted them into bins of width 0.01 Å. PMF surfaces were generated using a general and efficient multidimensional implementation of WHAM,[47,94] satisfying the following equation:[95]

$$W^{\mathrm{cm}}(\boldsymbol{\zeta}) = -\beta^{-1}\ln \rho(\boldsymbol{\zeta}) + C \tag{9}$$

where W^{cm} is the classical mechanical potential of mean force, $\boldsymbol{\zeta} = (\zeta_{\mathrm{asym}}, \zeta_{\mathrm{DAD}}, \zeta_{\mathrm{rehyb}})$ is the reaction coordinate vector, and ρ is the unbiased probability density. We note that in the current work we do not add the Jacobian of the transformation from locally rectilinear coordinates to generalized curvilinear coordinates.

Multidimensional WHAM. The WHAM approach is a histogram based method which combines the information from different biased free energy simulations while minimizing the statistical error.[47] The working equations for our WHAM calculations are provided in the Supporting Information.

In the current work, a multidimensional version of WHAM was implemented to allow the description of the multiple reaction coordinates. The WHAM code includes a general N-dimensional algorithm which facilitates the treatment of any dimension, similar to the umbrella sampling code implemented in CHARMM.[82,83] The N-dimensional reaction coordinate histogram, which is typically sparse, is stored as a dense one-dimensional vector, a feature which limits memory usage and significantly speeds up the WHAM calculation. The N-dimensional WHAM code is written in Fortran 95 and makes

extensive use of dynamic memory allocations to keep memory use to a minimum.

Additional features of the code include (i) instant f_k updating, which aids in convergence of the WHAM equations, (ii) restart capabilities which allow restarting WHAM jobs with intelligent initial guesses, such as f_k values of previous runs or alternatively an initial guess based on the average biasing potential used in a simulation, (iii) multidimensional smoothing of the free energy surface, (iv) rebinning capabilities which allow the generation of free energy surfaces with any bin size, and (v) slicing capabilities which allow the generation of free-energy iso-surfaces for easy interpretation of the multidimensional data.

The source code of the new multidimensional WHAM program is available as Supporting Information.

Finding the MFEP Using the String Method. The minimum-energy path (MEP) may be defined as the path orthogonal to the equipotential contours of a PES that connects the energy minima through the TS from which it slopes downward along the steepest descending lines in $3N - 6$ configurational space, where N is the number of nuclei in the reacting system.[96] In a system with potential energy, V, and at least two minima, the MEP will be a curve, γ, connecting these states, satisfying

$$(\nabla V)^{\perp}(\gamma) = 0 \tag{10}$$

where $(\nabla V)^{\perp}$ is the component of the gradient normal to γ. It follows that at each point along the MEP, the component of the force perpendicular to the path equals zero, and so the MEP is parallel to the gradient.[97] In more intuitive terms, the MEP is a global minimum over all paths connecting the RS to the PS.[97]

The string method[48−50] is an efficient approach for calculation of the MEP and thereby finding saddle points. It is classified as a chain-of-states method in the sense of employing a discretized series of nodes ("images") to represent the pathway in configuration space between given initial and final states, such as reaction and product configurations. It is also noteworthy that this method does not require the calculation of the Hessian matrix. In practice, an initial guess path is parametrized by a particular variable, typically a monotonic function of the normalized arc-length of the string.[97] The improved string method algorithm[50] employs a two-step procedure based on a time-splitting scheme: in the first step, the string is directed toward the MEP by evolving the images over some time interval, Δt. This is carried out by solving the following differential equation for each image on the guess curve, γ_i:

$$\frac{\partial \gamma_i}{\partial t} = -\nabla V(\gamma_i) \tag{11}$$

In the second step, which is applied occasionally, the images are redistributed along the string by enforcing an interpolation/reparametrization scheme, either by equal arc-length or by energy-weighted arc-length.

The utility of the string method in a collective variable space was demonstrated in the study of alanine dipeptide in a vacuum,[98] as well as in computing the MFEP for the hydrophobic collapse of a hydrated chain,[99] which involves over 10^5 atoms and 129 000 collective variables.

The original source code of the improved string method[50] (available for download online[100]) calculates the MEP, given a PES in an analytic functional form. It requires the initial and final states (expressed as coordinates), a time interval parameter, and a predetermined number of iterations requested for a particular run. Equation 11 is integrated using the forward Euler method, so that the new set of images after evolution, γ_i^{new}, is related to the older set, γ_i^{old}, by the following equation:

$$\gamma_i^{\text{new}} = \gamma_i^{\text{old}} - \Delta t \cdot \nabla V(\gamma_i^{\text{old}}) \tag{12}$$

We modified this code to allow multidimensional problems, as well as reading the multidimensional free energy surface as numerical data, which is the template of the output created by our WHAM program, thereby computing the MFEP. To this end, the force (gradient) was calculated numerically by evaluating the partial derivatives of the free energy with respect to each reaction coordinate. These data are classified and sorted into bins with the same widths used by the WHAM program to generate the free energy surface, so that each "image" on the path is assigned a set of indices which in turn specifies the related partial derivatives. In addition, to ensure proper convergence of the evolving path, we introduced a convergence criterion which calculates the root-mean-square deviation (RMSD) between matching points on the current path and its predecessor

$$\text{RMSD} = \sqrt{\frac{1}{N}\sum_{i=1}^{N} \|\gamma_i^{\text{new}} - \gamma_i^{\text{old}}\|^2} \tag{13a}$$

where N is the number of images on the string and γ_i is the ith image which may be expressed as a vector of the individual reaction coordinates (ζ_{asym}, ζ_{DAD}, ζ_{rehyb}). Therefore, eq 13a becomes

$$\text{RMSD} = \sqrt{\frac{1}{N}\sum_{i=1}^{N}\sum_{j=1}^{3} (\zeta_{i,j}^{\text{new}} - \zeta_{i,j}^{\text{old}})^2} \tag{13b}$$

Here, the inner summation index, j, runs over the aforementioned three coordinates. This quantity is evaluated after each iteration, prior to deciding whether to move on to the next iteration, until a user-defined threshold value is reached. The modified code was tested with the Müller−Brown PES[101] and the three-variable function $E(x, y, z) = 2y + y^2 + (y + 0.4x^2 + z^2)x^2 + 0.01z^2$ (considered as a reduced model of a higher-dimensional molecular PES corresponding to malonaldehyde-like systems[102]), both given in numerical forms.

Collective Reaction Coordinate. The MFEP obtained using the string method is a CRC, which is a function of the individual reaction coordinates, $\boldsymbol{\zeta} \equiv \boldsymbol{\zeta}(\{\zeta_i\})$. Practically, we define a scale such that the end point on the reactants side is determined as the reference image on the reaction path and given a zero value, where the rest of the images are equidistant in the three-dimensional reaction coordinate space. Therefore, the value of the nth image on the minimum free energy reaction path is equal to $\boldsymbol{\zeta}_n = (n - 1)\cdot\Delta\boldsymbol{\zeta}$ where $\Delta\boldsymbol{\zeta}$ is the distance between adjacent images along the string.

Transmission Coefficient Calculations. The transmission coefficient for the studied reaction was determined separately for the "$1D_{\text{asym}}$" and "$3D_{\text{asym}}$" sampling schemes based on the reactive flux correlation function approach,[13,14,103−105] which has been applied in studies of reactions in solutions[15,106−108] and enzymes.[107,109−110] In the calculation of the transmission coefficient for the two sampling schemes, the same trajectory pool was employed. In practice, we utilized the subtractive expression given in eq 3b to evaluate the time-dependent

Table 1. Comparative Analysis of Classical Free Energies (kcal/mol) of Reaction (ΔG_r) and Activation ($\Delta G^{\ddagger}$) and the Anti-Symmetric (AS) Stretch, Donor−Acceptor Distance (DAD), and Rehybridization at the Reactant, Transition, and Product States (RS, TS, PS) Computed with Different Umbrella Sampling Biasing Schemes[a]

biasing scheme	ΔG_r	$\Delta G^{\ddagger}$	property	RS	TS	PS
$1D_{asym}$	−6.4	15.9	AS stretch (Å)[b]	−1.65 ± 0.01	−0.09 ± 0.01	1.77 ± 0.01
			DAD (Å)[c]	3.79 ± 0.09	2.63 ± 0.06	3.66 ± 0.11
			rehybridization (Å)[c]	−1.16 ± 0.14	−0.06 ± 0.19	1.24 ± 0.06
$3D_{asym}$[d]	−6.4	16.0	AS stretch (Å)	−1.88 ± 0.02	−0.09 ± 0.02[e]	1.82 ± 0.02
			DAD (Å)	4.00 ± 0.02	2.63 ± 0.02	3.69 ± 0.02
			rehybridization (Å)	−1.18 ± 0.02	−0.05 ± 0.02[e]	1.22 ± 0.02
			CRC (Å)	0.00	2.79[f]	5.61
$3D_{DAD/rehyb}$[d,g]	−8.4	16.0	AS stretch (Å)	−1.89 ± 0.02	(−0.04 ± 0.02)	2.67 ± 0.02
			DAD (Å)	4.03 ± 0.02	(2.67 ± 0.02)	4.24 ± 0.02
			Rehybridization (Å)	−1.23 ± 0.02	(0.02 ± 0.02)	1.36 ± 0.02
			CRC (Å)	0.00	(2.72)	6.34

[a]The values of the collective reaction coordinate (CRC) are provided for the three-dimensional schemes. [b]Determined directly from the PMF. [c]Data were collected over all umbrella sampling molecular dynamics simulations ("windows") from reactants to products, and the calculated properties were sorted into bins of the antisymmetric stretch coordinate with a width of 0.01 Å and averaged over each bin. [d]Except where noted otherwise, data refer to the points ("images") on the minimum free energy reaction path generated by the string method, corresponding to local minima (RS, PS) and saddle point (TS). Fifty points were used to produce each path. [e]Determined by refinement of the approximate TS location. Starting with the string image corresponding to the highest free energy, the time-dependent transmission coefficient, $\kappa(t)$, was iteratively calculated until the rates of reduction in $\kappa_+(t)$ and increase in $\kappa_-(t)$ were balanced (i.e., $d\kappa_+(t)/dt \approx -d\kappa_-(t)/dt$). [f]Fitted by multiple regression analysis. [g]Values in parentheses are approximated with low confidence, due to the difficulty in sampling the dividing surface region.

transmission coefficient, $\kappa(t)$, where the transmission coefficient κ is the plateau value of $\kappa(t)$.[14]

We began with the trajectory recorded during the US simulations restrained at the TS region, as described above. Out of this pool of coordinates, we selected a subset of 100 configurations whose corresponding reaction coordinate(s) (either solely ζ_{asym} for the "$1D_{asym}$" scheme or all three coordinates together in the case of "$3D_{asym}$" scheme) were in the near vicinity of the TS. Specifically, we picked configurations that were within the TS volume element, i.e., $\zeta_i^{\ddagger} \pm \Delta\zeta_i/2$ where $\Delta\zeta_i$ = 0.01 and 0.04 Å for the 1D- and 3D-PMF cases, respectively (Table 1). For each of these TS configurations, we propagated 100 trajectories for 100 fs, amounting to 10^4 frames per time-step t. The initial velocities of all atoms were randomized to give a Maxwell−Boltzmann distribution, and the value of the reaction coordinate (or CRC, in the "$3D_{asym}$" scheme) in each frame was followed. Explicitly referring to K trajectories, we can rewrite eq 3b as

$$\kappa(t) = \frac{\sum_{i=1}^{K} \dot{\zeta}_i(0)\,\theta[\dot{\zeta}_i(0)]\,\theta[\zeta_i(t) - \zeta^{\ddagger}]}{\sum_{i=1}^{K} \dot{\zeta}_i(0)\,\theta[\dot{\zeta}_i(0)]} - \frac{\sum_{i=1}^{K} \dot{\zeta}_i(0)\,\theta[-\dot{\zeta}_i(0)]\,\theta[\zeta_i(t) - \zeta^{\ddagger}]}{\sum_{i=1}^{K} \dot{\zeta}_i(0)\,\theta[-\dot{\zeta}_i(0)]} \quad (14a)$$

where $\zeta_i(t)$ is the value of the reaction coordinate (or CRC) for the ith trajectory at time-step t, $\dot{\zeta}_i(0)$ is the corresponding velocity at t = 0, and θ is the Heaviside step function. Note that only positive velocities contribute to the summation in the minuend, whereas only negative velocities contribute to the summation in the subtrahend. We therefore sorted the frames into two individual subgroups, according to the direction of the initial velocities from which they originated. These subgroups correspond to the ensemble averages over the fractional equilibrium distributions, $\langle(...)\rangle_+$ and $\langle(...)\rangle_-$, described in eqs 3b and 3c. By simplifying the terms in eq 14a, it follows that

$$\kappa(t) = \frac{\sum_{i=1}^{N_+} \dot{\zeta}_i^{+}(0)\,\theta[\zeta_i(t) - \zeta^{\ddagger}]}{\sum_{i=1}^{N_+} \dot{\zeta}_i^{+}(0)} - \frac{\sum_{i=1}^{N_-} \dot{\zeta}_i^{-}(0)\,\theta[\zeta_i(t) - \zeta^{\ddagger}]}{\sum_{i=1}^{N_-} \dot{\zeta}_i^{-}(0)} = \kappa_+(t) - \kappa_-(t) \quad (14b)$$

which is the actual formula used to compute $\kappa(t)$. Here, N_+ and N_- are the numbers of trajectories with only initially positive or negative velocities, $\dot{\zeta}_i^{+}(0)$ and $\dot{\zeta}_i^{-}(0)$, respectively (so that K in eq 14a satisfies $K = N_+ + N_-$). In a compact form, the minuend and subtrahend in eq 14b will be referred to as $\kappa_+(t)$ and $\kappa_-(t)$. In both terms, the Heaviside step function is determined by keeping track of each frame and counting whether it is in the RS or PS well at time-step t (i.e., $\zeta_i(t) > \zeta^{\ddagger}$). All details related to the application of eq 14b in the $3D_{asym}$ scheme are given in the Supporting Information.

3. RESULTS AND DISCUSSION

Free Energy Simulations. Figure 1a provides a multidimensional depiction of the classical mechanical free energy landscape for the *ec*DHFR-catalyzed hydride transfer reaction, obtained with the new WHAM implementation. We employed the $3D_{asym}$ sampling scheme, in which a biasing potential was imposed on the antisymmetric stretch reaction coordinate, while the DAD and rehybridization coordinates were used as spectator coordinates. In this description, equidistant iso-surfaces are drawn along ζ_{asym} spanning the entire reaction coordinate, and each surface represents a "slice" of the free energy surface. The reaction pathway is depicted using color-mapped iso-contours atop each iso-surface. These iso-contours define both the progress of the reaction, in terms of all three reaction coordinates, and the relative free energy values associated with a given set of coordinates, as obtained from our QM/MM MD simulations. In addition, the resulting MFEP is seen as a curve passing through the iso-contours from the RS, via the dividing surface, to the PS.

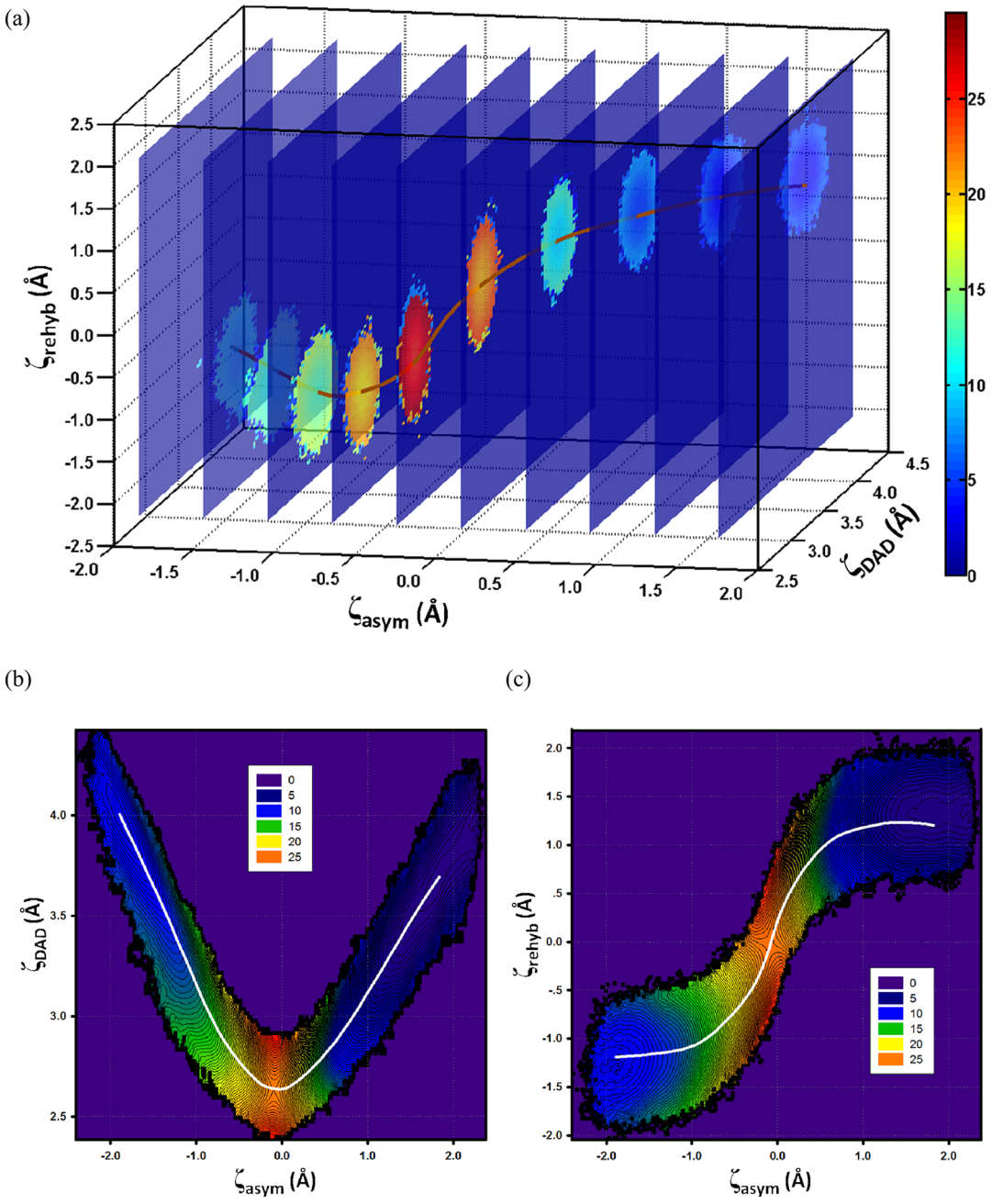

Figure 1. Classical (a) three- and (b, c) two-dimensional potential of mean force surfaces (kcal/mol) for the *ec*DHFR-catalyzed hydride transfer reaction as a function of the reaction coordinates as computed by applying biasing forces along the antisymmetric stretch coordinate, ζ_{asym}. Associated minimum free energy paths (brown- and white-colored curves in a and in b and c, respectively) are also shown.

In Figure 1b and c, we present a pair of two-dimensional classical PMFs, derived from the same probability density data used to form the full three-dimensional PMF discussed above, utilizing the new WHAM implementation. In particular, the left panel (Figure 1b) provides the free energy surface as a function of the antisymmetric stretch and DAD coordinates (abscissa and ordinate, respectively), while averaging the contributions of the rehybridization coordinate. The free energy in the right panel (Figure 1c) is described in terms of the antisymmetric stretch and rehybridization coordinates, this time averaged over the DAD coordinate. We stress that no biasing potentials were applied to the rehybridization or DAD coordinates in the $3D_{asym}$ sampling scheme. There are some notable findings that can be inferred from these PMF surfaces. First, the variation of the DAD with the antisymmetric stretch coordinate (Figure 1b) is roughly parabolic, in agreement with previous computational studies,[62,67,92] reaching its shortest distance of ca. 2.63 Å at the TS. That is, the shortening of the DAD is coupled to the hydride transfer as expected. Interestingly, moderate fluctuations about this optimal DAD (ca. ± 0.1 Å) result in only a minor increase in free energy, suggesting that the classical dividing surface area tolerates a relatively wide range of DAD configurations. In comparison to the DAD obtained from classical simulations, the DAD distances are somewhat greater when treating the transferring hydride as a quantum particle (Figure S4; see ref 51 for calculation details). In the case of a single quantized hydride, the DAD is 2.66 Å, while quantizing deuteride yields a DAD of 2.65 Å. Second, the rehybridization

dx.doi.org/10.1021/ct300235k | J. Chem. Theory Comput. 2012, 8, 2484−2496

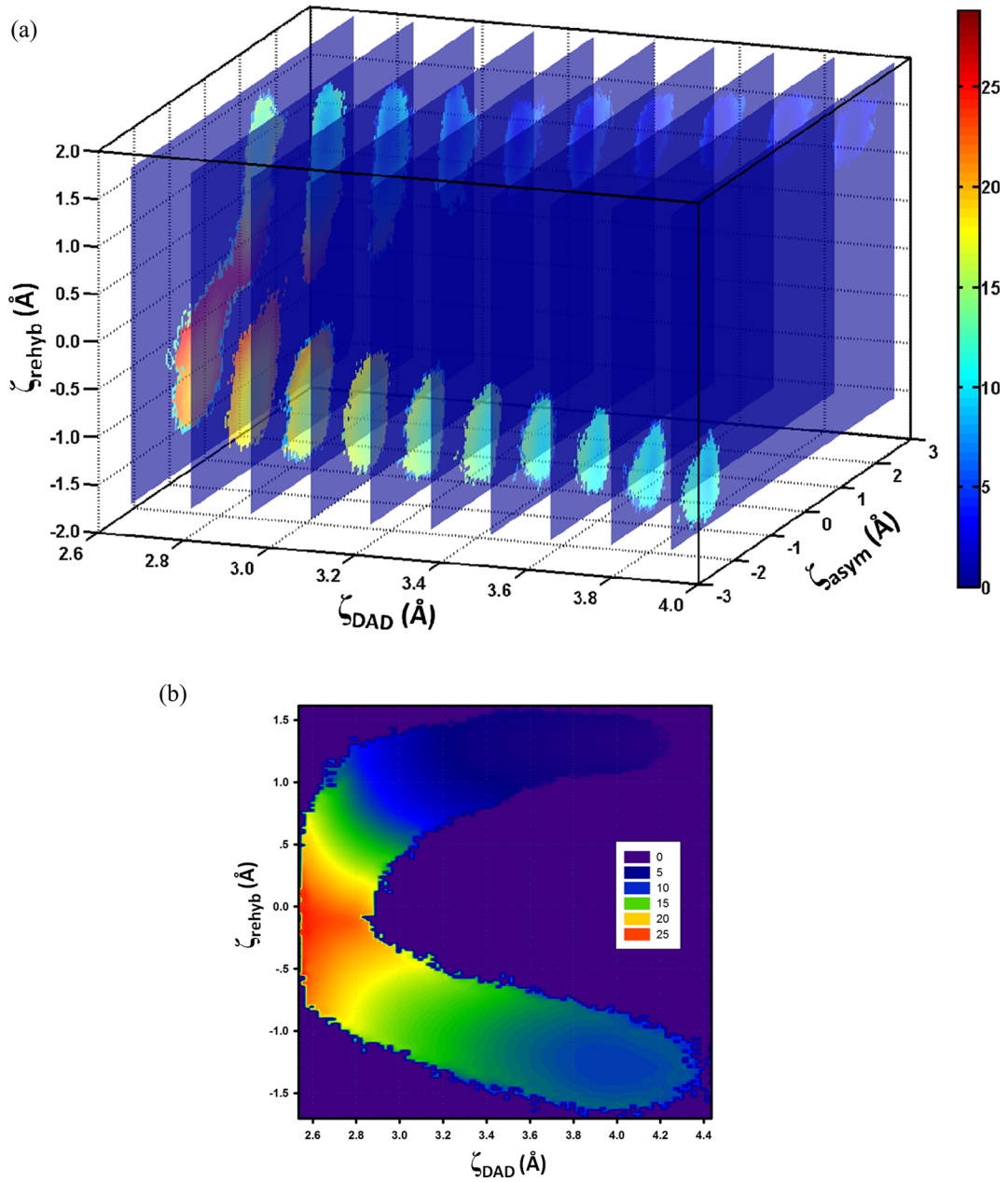

Figure 2. Classical (a) three- and (b) two-dimensional potential of mean force surfaces (kcal/mol) for the *ec*DHFR-catalyzed hydride transfer reaction as a function of the reaction coordinates as computed by applying biasing forces along the donor−acceptor distance (DAD) and rehybridization coordinates, ζ_{DAD} and ζ_{rehyb}.

coordinate does not progress linearly with respect to the antisymmetric stretch coordinate (Figure 1c). The sigmoidal shape of the PMF surface (and the MFEP curve) implies that the change in the hybridization states of the donor and acceptor carbons lags behind the migration of the hydride at its very beginning (RS region) and end (PS region). On the other hand, the rehybridization exhibits its fastest change around the dividing surface (TS region). The nonlinear relationship between these two reaction coordinates is consistent with Pu et al.'s study on *ec*DHFR,[42] which found that although the hydride transfer is concerted as a whole, the individual rehybridizations of the donating and accepting carbons progress asynchronously. This is manifested by the variation of their sum along the antisymmetric stretch coordinate (referred to as nonconservation of the "hybridization looseness perpendicular to the reaction coordinate"). The variation of the hybridization states of the donor (C4N) and acceptor (C6) carbons and their sum along the antisymmetric stretch coordinate, ζ_{asym}, are presented in Figure S2, and the reaction path, in terms of the mutual progress of hybridization states, χ, of the donor (C4N) and acceptor (C6) carbons is presented in Figure S3. In our current study, the rehybridization reaction coordinate is expressed as the difference between the individual hybridization states (rather than their sum), and we can clearly notice that at the saddle point its value is approaching zero ($\zeta_{rehyb} = -0.05$ Å), suggesting that the donor and acceptor carbons adopt the same intermediate hybridization state, in line with Pu et al.'s findings with respect to the crossing over of the hybridization curves at the transition state.[42] Interestingly, the free energy change is smaller in the region around the TS where the

dx.doi.org/10.1021/ct300235k | J. Chem. Theory Comput. 2012, 8, 2484−2496

rehybridization is the greatest, while the free energy change is greater in the regions where the antisymmetric stretch coordinate shows the greatest variation. This suggests that less force is required to drive rehybridization than hydride transfer, or in other words, the rehybridization coordinate is a softer degree of freedom than the antisymmetric stretch coordinate. Finally, the free energies of reaction and activation inferred from the 2D surfaces (without nuclear quantum correction), −6.4 and 16.0 kcal/mol, respectively, are in good agreement with the results for the "$1D_{asym}$" scheme reported in our introductory study[51] (Table 1) and with the experimental data[52] (−4.4 and 13.4 kcal/mol).

In contrast to the relative ease with which the free energy landscape of the hydride transfer reaction was sampled using the $3D_{asym}$ biasing scheme, the biasing of the DAD and rehybridization reaction coordinates only was more challenging, especially at the dividing surface and its surroundings. Specifically, the antisymmetric stretch coordinate, treated as a spectator coordinate, was not well sampled at the TS. The multidimensional free energy surface generated by the $3D_{DAD/rehyb}$ scheme is shown in Figure 2a, where the iso-surfaces are plotted across the DAD reaction coordinate. Inspection of this sequence of iso-surfaces reveals a pair of iso-contours whose relative proximity is varied with change of the DAD, a trend that can be interpreted in terms of the parabolic-like characteristics of the ζ_{DAD} with respect to ζ_{asym}. At the upper limit of ζ_{DAD} (3.7−4.0 Å), the positions of the two contours on the iso-surface and their associated free energies reflect the local minima (i.e., RS and PS). As the DAD coordinate becomes shorter, ζ_{asym} and ζ_{rehyb} progress monotonically toward the TS (ζ_{DAD} = 2.6−2.7 Å). Figure 2b describes the two-dimensional PMF as a function of the DAD and rehybridization reaction coordinates, averaged over ζ_{asym}, which is the monitoring coordinate in the $3D_{DAD/rehyb}$ scheme. We note that the difficulty in sampling the TS with the $3D_{DAD/rehyb}$ scheme is due to the nature of the rehybridization coordinate, which is a softer degree of freedom than the antisymmetric stretch coordinate. This makes the absolute determination of the saddle point difficult (Table 1). We further note that the current simulations are classical and that quantizing the transferring hydride would likely enhance the sampling at the TS due to tunneling. Although it is tempting to describe the reaction in terms of the DAD and rehybridization coordinates exclusively (without exerting forces on the migrating H-atom), the issues described above suggest that this coordinate is not adequately robust in itself to promote the hydride transfer, in the absence of nuclear quantum effects. However, this coordinate may readily be used in conjunction with direct quantum dynamics simulations.[67] It follows that the geometric information provided by the antisymmetric stretch coordinate is still necessary to sufficiently sample the TS region in classical simulations.

Table 1 compares the classical free energies and the antisymmetric stretch, DAD, and rehybridization reaction coordinates at the reactant, transition, and product states calculated with the different biasing schemes. The values of the CRC at these states are given as well for the three-dimensional schemes. In general, comparison of the geometric features of the RS, TS, and PS reveals that the $1D_{asym}$ and $3D_{asym}$ schemes give similar values. However, in the one-dimensional scheme there is a significant spread in the DAD and rehybridization coordinates around the average values (as manifested by the relatively large standard deviations). Additionally, there is some uncertainty associated with the location of the RS and PS due to the shallow nature of the free energy minima in the respective PMFs. Finally, a concise description of the MFEPs for the two 3D biasing schemes in terms of the CRC is illustrated in Figure 3. MFEP projections onto individual reaction coordinates are provided in the Supporting Information.

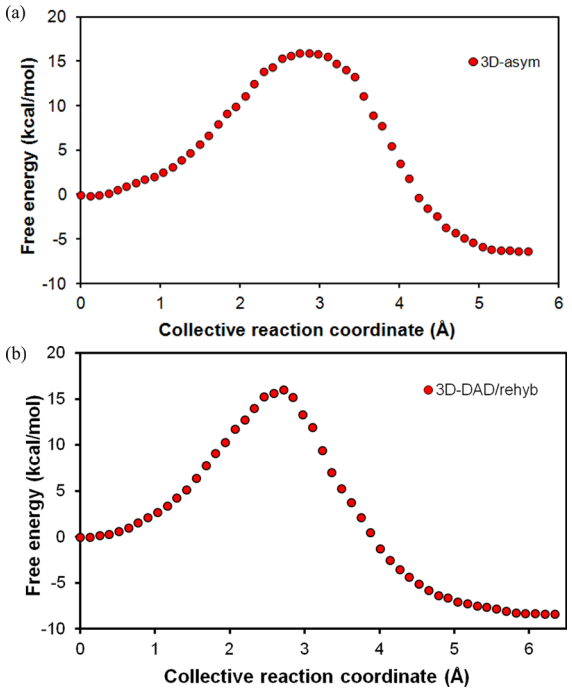

Figure 3. The minimum free energy paths (kcal/mol) for the hydride transfer reaction in *ec*DHFR as a function of the collective reaction coordinate based on biased sampling of the (a) antisymmetric stretch coordinate ($3D_{asym}$) or the (b) DAD and rehybridization coordinates ($3D_{DAD/rehyb}$). The red points on each curve represent an optimized series of 50 images along the path obtained by the string method.

Transmission Coefficient Calculations. Figure 4 shows the time-dependent classical transmission coefficients for the H^--transfer reaction in *ec*DHFR calculated with the $1D_{asym}$ and $3D_{asym}$ reaction coordinates. Generally speaking, by definition, the function $\kappa(t)$ is equal to 1 at the commencement of the active dynamics, when all trajectories are productive ($\kappa_+(0)$ =

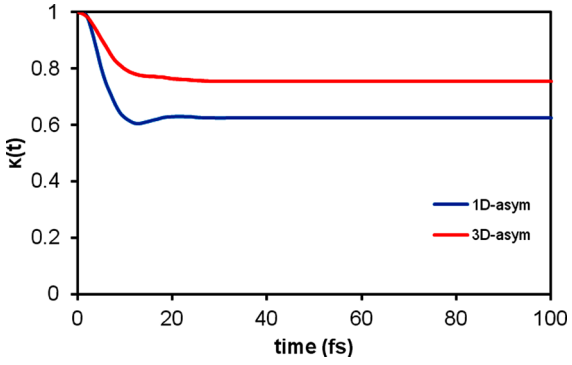

Figure 4. The time-dependent transmission coefficient, $\kappa(t)$, for the hydride transfer reaction in *ec*DHFR, computed on the basis of trajectories produced with one-dimensional ($1D_{asym}$, blue curve) and three-dimensional ($3D_{asym}$, red curve) umbrella sampling simulations.

dx.doi.org/10.1021/ct300235k | J. Chem. Theory Comput. 2012, 8, 2484−2496

1) and none are headed in the opposite direction toward the RS ($\kappa_-(0) = 0$). This is followed by a short decay of the $\kappa(t)$ curve to a plateau, corresponding to a relaxation period during which the trajectories may recross the transition state until they all settle into either the RS or PS.[110] In both reaction coordinate schemes, $\kappa(t)$ approaches the plateau value within 25 fs, similar to the finding of Miller et al.[67] Specifically, when the reaction coordinate is exclusively defined by the $1D_{asym}$ antisymmetric stretch coordinate, the computed κ is 0.63, whereas it is 0.76 using the $3D_{asym}$ CRC description (Figure 4). This difference amounts to 0.1 kcal/mol, thus bringing the computed rate constants using the $1D_{asym}$ and $3D_{asym}$ schemes into perfect agreement (Table 1). For the sake of comparison, Garcia-Viloca et al.[61] employed a QM/MM PES with a simple valence bond correction and ensemble-averaged variational transition state theory with multidimensional tunneling (EA-VTST/MT) to compute the transmission coefficient for the *ec*DHFR reaction, which accounts for dynamical barrier recrossing. The reaction coordinate used in that study was the antisymmetric stretch coordinate, and the transmission coefficient obtained (for the all-protium isotopomer) was 0.75. On the other hand, Agarwal et al.[60] found a transmission coefficient of 0.80 using EVB PES where the reaction coordinate was defined as the energy gap between the reactant and product diabatic states. Miller and co-workers found classical and quantum transmission coefficients of 0.89 and 0.66, respectively, employing the same PES as Agarwal et al.[67] We bear in mind that the transmission coefficient depends on the choice of the reaction coordinate,[14] as well as the potential energy surface employed and simulation details. Referring back to our results, the higher transmission coefficient obtained for the $3D_{asym}$ scheme inevitably suggests that the inclusion of simple geometric reorganization coordinates as part of the reaction coordinate, in addition to the standard antisymmetric stretch coordinate, provides a better description of the dividing surface with reduced recrossing.

4. CONCLUSIONS

In the current work, we derive a new collective reaction coordinate that is readily incorporated into MO- or DFT-based hybrid QM/MM free energy simulations. The coordinate is composed of the traditional antisymmetric stretch coordinate as a distinguished reaction coordinate, while the DAD and rehybridization coordinates represent parts of the Marcus inner-sphere reorganization coordinate. This composite collective reaction coordinate is employed in multidimensional umbrella sampling simulations, and the resulting data are combined with a new multidimensional WHAM code. The search for the minimum free energy path in the multidimensional space is guided by use of the string method which iteratively improves the minimum free energy path. The computed classical recrossing transmission coefficients show that the combined collective coordinate yields less recrossing than the traditional antisymmetric stretch coordinate. Additionally, the collective reaction coordinate provides important intuitive information regarding the correlation between reaction free energy, DAD, rehybridization, and reaction progress.

■ ASSOCIATED CONTENT

Ⓢ Supporting Information

Projections of the MFEP onto each reaction coordinate based on the free energy surface obtained with the $3D_{asym}$ biasing scheme, free energy surfaces with nuclear quantum correction, description of the WHAM equations used in this work, calculation of time-dependent transmission coefficient with a multidimensional reaction coordinate, an example of a CHARMM input script file for running multidimensional umbrella sampling simulations with biasing forces on the antisymmetric stretch reaction coordinate ($3D_{asym}$), and the multidimensional WHAM code. This material is available free of charge via the Internet at http://pubs.acs.org.

■ AUTHOR INFORMATION

Corresponding Author

*E-mail: majort@biu.ac.il.

Notes

The authors declare no competing financial interest.

■ ACKNOWLEDGMENTS

This work has been supported by the Israel Science Foundation and the United States−Israel Binational Science Foundation (Grant # 2007256). We thank Prof. Kenneth Kay for helpful discussions, and Ms. Karin Povolozki for her assistance in adapting the string method algorithm to numerical data input.

■ REFERENCES

(1) Eyring, H.; Stearn, A. E. The Application of the Theory of Absolute Reacton Rates to Proteins. *Chem. Rev.* **1939**, *24*, 253.
(2) Truhlar, D. G.; Hase, W. L.; Hynes, J. T. Current Status of Transition-State Theory. *J. Phys. Chem.* **1983**, *87*, 2664.
(3) Wynne-Jones, W. F. K.; Eyring, H. The Absolute Rate of Reactions in Condensed Phases. *J. Chem. Phys.* **1935**, *3*, 492.
(4) Benkovic, S. J.; Hammes-Schiffer, S. A Perspective on Enzyme Catalysis. *Science* **2003**, *301*, 1196.
(5) Garcia-Viloca, M.; Gao, J.; Karplus, M.; Truhlar, D. G. How Enzymes Work: Analysis by Modern Rate Theory and Computer Simulations. *Science* **2004**, *303*, 186.
(6) Olsson, M. H. M.; Mavri, J.; Warshel, A. Transition state theory can be used in studies of enzyme catalysis: lessons from simulations of tunnelling and dynamical effects in lipoxygenase and other systems. *Philos. Trans. R. Soc. London, Ser. B* **2006**, *361*, 1417.
(7) Northrup, S. H.; Pear, M. R.; Lee, C. Y.; McCammon, J. A.; Karplus, M. Dynamical theory of activated processes in globular proteins. *Proc. Natl. Acad. Sci. U. S. A.* **1982**, *79*, 4035.
(8) Hinsen, K.; Roux, B. Potential of mean force and reaction rates for proton transfer in acetylacetone. *J. Chem. Phys.* **1997**, *106*, 3567.
(9) Gao, J.; Ma, S.; Major, D. T.; Nam, K.; Pu, J.; Truhlar, D. G. Mechanisms and Free Energies of Enzymatic Reactions. *Chem. Rev.* **2006**, *106*, 3188.
(10) Pu, J.; Gao, J.; Truhlar, D. G. Multidimensional Tunneling, Recrossing, and the Transmission Coefficient for Enzymatic Reactions. *Chem. Rev.* **2006**, *106*, 3140.
(11) Torrie, G. M.; Valleau, J. P. Nonphysical sampling distributions in Monte Carlo free-energy estimation: Umbrella sampling. *J. Comput. Phys.* **1977**, *23*, 187.
(12) Kästner, J. Umbrella sampling. *WIREs Comput. Mol. Sci.* **2011**, *1*, 932.
(13) Chandler, D. Roles of classical dynamics and quantum dynamics on activated processes occurring in liquids. *J. Stat. Phys.* **1986**, *42*, 49.
(14) Berne, B. J.; Borkovec, M.; Straub, J. E. Classical and modern methods in reaction rate theory. *J. Phys. Chem.* **1988**, *92*, 3711.
(15) Gertner, B. J.; Wilson, K. R.; Hynes, J. T. Nonequilibrium solvation effects on reaction rates for model S_N2 reactions in water. *J. Chem. Phys.* **1989**, *90*, 3537.
(16) Weinan, E.; Vanden-Eijnden, E. Transition-Path Theory and Path-Finding Algorithms for the Study of Rare Events. *Annu. Rev. Phys. Chem.* **2010**, *61*, 391.

(17) Dellago, C.; Bolhuis, P. G.; Chandler, D. On the calculation of reaction rate constants in the transition path ensemble. *J. Chem. Phys.* **1999**, *110*, 6617.
(18) Roston, D.; Kohen, A. Elusive transition state of alcohol dehydrogenase unveiled. *Proc. Natl. Acad. Sci. U. S. A.* **2010**, *107*, 9572.
(19) Henkelman, G.; Uberuaga, B. P. A climbing image nudged elastic band method for finding saddle points and minimum energy paths. *J. Chem. Phys.* **2000**, *113*, 9901.
(20) Henkelman, G.; Jonsson, H. Improved tangent estimate in the nudged elastic band method for finding minimum energy paths and saddle points. *J. Chem. Phys.* **2000**, *113*, 9978.
(21) Truhlar, D. G.; Gao, J.; Alhambra, C.; Garcia-Viloca, M.; Corchado, J.; Sánchez, M. L.; Villà, J. The Incorporation of Quantum Effects in Enzyme Kinetics Modeling. *Acc. Chem. Res.* **2002**, *35*, 341.
(22) Rosta, E.; Woodcock, H. L.; Brooks, B. R.; Hummer, G. Artificial reaction coordinate "tunneling" in free-energy calculations: The catalytic reaction of RNase H. *J. Comput. Chem.* **2009**, *30*, 1634.
(23) Eyring, H. The activated complex in chemical reactions. *J. Chem. Phys.* **1935**, *3*, 107.
(24) Gao, J.; Ma, S.; Major, D. T.; Nam, K.; Pu, J.; Truhlar, D. G. Mechanisms and Free Energies of Enzymatic Reactions. *Chem. Rev.* **2006**, *106*, 3188.
(25) Chandrasekhar, J.; Smith, S. F.; Jorgensen, W. L. S_N2 reaction profiles in the gas phase and aqueous solution. *J. Am. Chem. Soc.* **1984**, *106*, 3049.
(26) Gao, J. Hybrid quantum and molecular mechanical simulations: An alternative avenue to solvent effects in organic chemistry. *Acc. Chem. Res.* **1996**, *29*, 298.
(27) Bruice, T. C.; Benkovic, S. J. Chemical basis for enzyme catalysis. *Biochemistry* **2000**, *39*, 6267.
(28) Marcus, R. A. On the theory of oxidation-reduction reactions involving electron transfer. I. *J. Chem. Phys.* **1956**, *24*, 966.
(29) Marcus, R. A.; Sutin, N. Electron transfers in chemistry and biology. *Biochim. Biophys. Acta, Rev. Bioenerg.* **1985**, *811*, 265.
(30) Warshel, A. *Computer Modeling of Chemical Reactions in Enzymes*; Wiley: New York, 1991.
(31) Villa, J.; Warshel, A. Energetics and Dynamics of Enzymatic Reactions. *J. Phys. Chem. B* **2001**, *105*, 7887.
(32) Mo, Y.; Gao, J. An initio QM/MM simulations with a molecular orbital-valence bond (MOVB) method: application to an S_N2 reaction in water. *J. Comput. Chem.* **2000**, *21*, 1458.
(33) Mo, Y.; Gao, J. An ab-initio molecular orbital-valence bond (MOVB) method for simulating chemical reactions in solution. *J. Phys. Chem. A* **2000**, *104*, 3012.
(34) Mones, L.; Kulhánek, P.; Simon, I.; Laio, A.; Fuxreiter, M. The Energy Gap as a Universal Reaction Coordinate for the Simulation of Chemical Reactions. *J. Phys. Chem. B* **2009**, *113*, 7867.
(35) Schenter, G. K.; Garrett, B. C.; Truhlar, D. G. The Role of Collective Solvent Coordinates and Nonequilibrium Solvation in Charge-Transfer Reactions. *J. Phys. Chem. B* **2001**, *105*, 9672.
(36) Sharir-Ivry, A.; Shurki, A. VB/MM - The Validity of the Underlying Approximations. *J. Phys. Chem. B* **2008**, *112*, 12491.
(37) Sharir-Ivry, A.; Crown, H. A.; Wu, W.; Shurki, A. Density Embedded VB/MM: A Hybrid ab Initio VB/MM with Electrostatic Embedding. *J. Phys. Chem. A* **2008**, *112*, 2489.
(38) Hu, H.; Yang, W. Elucidating Solvent Contributions to Solution Reactions with Ab Initio QM/MM Methods. *J. Phys. Chem. B* **2010**, *114*, 2755.
(39) Ruiz-Pernía, J. J.; Martí, S.; Moliner, V.; Tuñón, I. A Novel Strategy to Study Electrostatic Effects in Chemical Reactions: Differences between the Role of Solvent and the Active Site of Chalcone Isomerase in a Michael Addition. *J. Chem. Theory Comput.* **2012**, *8*, 1532.
(40) Haddon, R. C.; Chow, S. Y. Hybridization as a Metric for the Reaction Coordinate of Chemical Reactions. *J. Am. Chem. Soc.* **1998**, *120*, 10494.
(41) Haddon, R. C.; Chow, S. Y. Hybridization as a metric for the reaction coordinate of the chemical reaction. Concert in chemical reactions. *Pure Appl. Chem.* **1999**, *71*, 289.
(42) Pu, J.; Ma, S.; Garcia-Viloca, M.; Gao, J.; Truhlar, D. G.; Kohen, A. Nonperfect Synchronization of Reaction Center Rehybridization in the Transition State of the Hydride Transfer Catalyzed by Dihydrofolate Reductase. *J. Am. Chem. Soc.* **2005**, *127*, 14879.
(43) Major, D. T.; York, D. M.; Gao, J. L. Solvent polarization and kinetic isotope effects in nitroethane deprotonation and implications to the nitroalkane oxidase reaction. *J. Am. Chem. Soc.* **2005**, *127*, 16374.
(44) Major, D. T.; Heroux, A.; Orville, A. M.; Valley, M. P.; Fitzpatrick, P. F.; Gao, J. Differential quantum tunneling contributions in nitroalkane oxidase catalyzed and the uncatalyzed proton transfer reaction. *Proc. Natl. Acad. Sci. U.S.A.* **2009**, *106*, 20734.
(45) Kiefer, P. M.; Hynes, J. T. Theoretical aspects of tunneling proton transfer reactions in a polar environment. *J. Phys. Org. Chem.* **2010**, *23*, 632.
(46) Nagel, Z. D.; Klinman, J. P. A 21st century revisionist's view at a turning point in enzymology. *Nat. Chem. Biol.* **2009**, *5*, 543.
(47) Kumar, S.; Rosenberg, J. M.; Bouzida, D.; Swendsen, R. H.; Kollman, P. A. The weighted histogram analysis method for free-energy calculations on biomolecules. I. The method. *J. Comput. Chem.* **1992**, *13*, 1011.
(48) E, W.; Ren, W.; Vanden-Eijnden, E. String method for the study of rare events. *Phys. Rev. B* **2002**, *66*, 052301.
(49) Ren, W. Higher order string method for finding minimum energy paths. *Commun. Math. Sci.* **2003**, *1*, 377.
(50) E, W.; Ren, W.; Vanden-Eijnden, E. Simplified and improved string method for computing the minimum energy paths in barrier-crossing events. *J. Chem. Phys.* **2007**, *126*, 164103.
(51) Doron, D.; Major, D. T.; Kohen, A.; Thiel, W.; Wu, X. Hybrid Quantum and Classical Simulations of the Dihydrofolate Reductase Catalyzed Hydride Transfer Reaction on an Accurate Semi-Empirical Potential Energy Surface. *J. Chem. Theory Comput.* **2011**, *7*, 3420.
(52) Fierke, C. A.; Johnson, K. A.; Benkovic, S. J. Construction and Evaluation of the Kinetic Scheme Associated with Dihydrofolate Reductase from *Escherichia coli*. *Biochemistry* **1987**, *26*, 4085.
(53) Rajagopalan, P.; Lutz, S.; Benkovic, S. Coupling interactions of distal residues enhance dihydrofolate reductase catalysis: mutational effects on hydride transfer rates. *Biochemistry* **2002**, *41*, 12618.
(54) Sikorski, R. S.; Wang, L.; Markham, K. A.; Rajagopalan, P. T. R.; Benkovic, S. J.; Kohen, A. Tunneling and coupled motion in the *Escherichia coli* dihydrofolate reductase catalysis. *J. Am. Chem. Soc.* **2004**, *126*, 4778.
(55) Wang, L.; Tharp, S.; Selzer, T.; Benkovic, S. J.; Kohen, A. Effects of a Distal Mutation on Active Site Chemistry. *Biochemistry* **2006**, *45*, 1383.
(56) Wang, L.; Goodey, N. M.; Benkovic, S. J.; Kohen, A. Coordinated effects of distal mutations on environmentally coupled tunneling in dihydrofolate reductase. *Proc. Natl. Acad. Sci. U. S. A.* **2006**, *103*, 15753.
(57) Wang, L.; Goodey, N. M.; Benkovic, S. J.; Kohen, A. The role of enzyme dynamics and tunnelling in catalysing hydride transfer: studies of distal mutants of dihydrofolate reductase. *Philos. Trans. R. Soc. London, Ser. B* **2006**, *361*, 1307.
(58) Stojković, V.; Perissinotti, L. L.; Lee, J.; Benkovic, S. J.; Kohen, A. The effect of active-site isoleucine to alanine mutation on the DHFR catalyzed hydride-transfer. *Chem. Commun.* **2010**, *46*, 8974.
(59) Stojković, V.; Perissinotti, L. L.; Willmer, D.; Benkovic, S. J.; Kohen, A. Effects of the Donor−Acceptor Distance and Dynamics on Hydride Tunneling in the Dihydrofolate Reductase Catalyzed Reaction. *J. Am. Chem. Soc.* **2012**, *134*, 1738.
(60) Agarwal, P. K.; Billeter, S. R.; Hammes-Schiffer, S. Nuclear quantum effects and enzyme dynamics in dihydrofolate reductase catalysis. *J. Phys. Chem. B* **2002**, *106*, 3283.
(61) Garcia-Viloca, M.; Truhlar, D. G.; Gao, J. Reaction-Path Energetics and Kinetics of the Hydride Transfer Reaction Catalyzed by Dihydrofolate Reductase. *Biochemistry* **2003**, *42*, 13558.
(62) Thorpe, I. F.; Brooks, C. L., III Barriers to Hydride Transfer in Wild Type and Mutant Dihydrofolate Reductase from *E. coli*. *J. Phys. Chem. B* **2003**, *107*, 14042.

(63) Hammes-Schiffer, S. Quantum−classical simulation methods for hydrogen transfer in enzymes: a case study of dihydrofolate reductase. *Curr. Opin. Struct. Biol.* **2004**, *14*, 192.
(64) Pu, J.; Ma, S.; Gao, J.; Truhlar, D. G. Small Temperature Dependence of the Kinetic Isotope Effect for the Hydride Transfer Reaction Catalyzed by *Escherichia coli* Dihydrofolate Reductase. *J. Phys. Chem. B* **2005**, *109*, 8551.
(65) Liu, H.; Warshel, A. The Catalytic Effect of Dihydrofolate Reductase and Its Mutants Is Determined by Reorganization Energies. *Biochemistry* **2007**, *46*, 6011.
(66) Liu, H.; Warshel, A. Origin of the Temperature Dependence of Isotope Effects in Enzymatic Reactions: The Case of Dihydrofolate Reductase. *J. Phys. Chem. B* **2007**, *111*, 7852.
(67) Boekelheide, N.; Salomón-Ferrer, R.; Miller, T. F. Dynamics and dissipation in enzyme catalysis. *Proc. Natl. Acad. Sci. U. S. A.* **2011**, *108*, 16159.
(68) Engel, H.; Doron, D.; Kohen, A.; Major, D. T. Momentum Distribution as a Fingerprint of Quantum Delocalization in Enzymatic Reactions: Open-Chain Path-Integral Simulations of Model Systems and the Hydride Transfer in Dihydrofolate Reductase. *J. Chem. Theory Comput.* **2012**, *8*, 1223.
(69) Sawaya, M. R.; Kraut, J. Loop and Subdomain Movements in the Mechanism of *Escherichia coli* Dihydrofolate Reductase: Crystallographic Evidence. *Biochemistry* **1997**, *36*, 586.
(70) Chen, Y. Q.; Kraut, J.; Blakley, R. L.; Callender, R. Determination by Raman Spectroscopy of the pK_a of N5 of Dihydrofolate Bound to Dihydrofolate Reductase: Mechanistic Implications. *Biochemistry* **1994**, *33*, 7021.
(71) Chen, Y.; Kraut, J.; Callender, R. pH-dependent conformational changes in *Escherichia coli* dihydrofolate reductase revealed by Raman difference spectroscopy. *Biophys. J.* **1997**, *72*, 936.
(72) Deng, H.; Callender, R. Structure of Dihydrofolate When Bound to Dihydrofolate Reductase. *J. Am. Chem. Soc.* **1998**, *120*, 7730.
(73) Warshel, A.; Levitt, M. Theoretical studies of enzymic reactions: Dielectric, electrostatic and steric stabilization of the carbonium ion in the reaction of lysozyme. *J. Mol. Biol.* **1976**, *103*, 227.
(74) Gao, J., Methods and Applications of Combined Quantum Mechanical and Molecular Mechanical Potentials. In *Rev. Comput. Chem.*; Lipkowitz, K. B., Boyd, D. B., Eds.; VCH Publishers: New York, 1995; Vol. 7, p 119.
(75) Gao, J.; Thompson, M. A. *Combined Quantum Mechanical and Molecular Mechanical Methods*; American Chemical Society: Washington, DC, 1998; Vol. *712*.
(76) Dewar, M. J. S.; Zoebisch, E. G.; Healy, E. F.; Stewart, J. J. P. AM1: a new general purpose quantum mechanical molecular model. *J. Am. Chem. Soc.* **1985**, *107*, 3902.
(77) MacKerell, A. D.; Bashford, D.; Bellott; Dunbrack, R. L.; Evanseck, J. D.; Field, M. J.; Fischer, S.; Gao, J.; Guo, H.; Ha, S.; Joseph-McCarthy, D.; Kuchnir, L.; Kuczera, K.; Lau, F. T. K.; Mattos, C.; Michnick, S.; Ngo, T.; Nguyen, D. T.; Prodhom, B.; Reiher, W. E.; Roux, B.; Schlenkrich, M.; Smith, J. C.; Stote, R.; Straub, J.; Watanabe, M.; Wiorkiewicz-Kuczera, J.; Yin, D.; Karplus, M. All-Atom Empirical Potential for Molecular Modeling and Dynamics Studies of Proteins. *J. Phys. Chem. B* **1998**, *102*, 3586.
(78) MacKerell, A. D.; Banavali, N.; Foloppe, N. Development and current status of the CHARMM force field for nucleic acids. *Biopolymers* **2000**, *56*, 257.
(79) MacKerell, A. D.; Feig, M.; Brooks, C. L., III. Extending the treatment of backbone energetics in protein force fields: Limitations of gas-phase quantum mechanics in reproducing protein conformational distributions in molecular dynamics simulations. *J. Comput. Chem.* **2004**, *25*, 1400.
(80) Jorgensen, W. L.; Chandrasekhar, J.; Madura, J. D.; Impey, R. W.; Klein, M. L. Comparison of simple potential functions for simulating liquid water. *J. Chem. Phys.* **1983**, *79*, 926.
(81) Gao, J. Toward a Molecular Orbital Derived Empirical Potential for Liquid Simulations. *J. Phys. Chem. B* **1997**, *101*, 657.
(82) Brooks, B. R.; Bruccoleri, R. E.; Olafson, B. D.; States, D. J.; Swaminathan, S.; Karplus, M. CHARMM: A program for macromolecular energy, minimization, and dynamics calculations. *J. Comput. Chem.* **1983**, *4*, 187.
(83) Brooks, B. R.; Brooks, C. L., III; MacKerell, A. D., Jr.; Nilsson, L.; Petrella, R. J.; Roux, B.; Won, Y.; Archontis, G.; Bartels, C.; Boresch, S.; Caflisch, A.; Caves, L.; Cui, Q.; Dinner, A. R.; Feig, M.; Fischer, S.; Gao, J.; Hodoscek, M.; Im, W.; Kuczera, K.; Lazaridis, T.; Ma, J.; Ovchinnikov, V.; Paci, E.; Pastor, R. W.; Post, C. B.; Pu, J. Z.; Schaefer, M.; Tidor, B.; Venable, R. M.; Woodcock, H. L.; Wu, X.; Yang, W.; York, D. M.; Karplus, M. CHARMM: The biomolecular simulation program. *J. Comput. Chem.* **2009**, *30*, 1545.
(84) Nam, K.; Gao, J.; York, D. M. An Efficient Linear-Scaling Ewald Method for Long-Range Electrostatic Interactions in Combined QM/MM Calculations. *J. Chem. Theory Comput.* **2005**, *1*, 2.
(85) Andersen, H. C. Molecular dynamics simulations at constant pressure and/or temperature. *J. Chem. Phys.* **1980**, *72*, 2384.
(86) Feller, S. E.; Zhang, Y.; Pastor, R. W.; Brooks, B. R. Constant pressure molecular dynamics simulation: The Langevin piston method. *J. Chem. Phys.* **1995**, *103*, 4613.
(87) Hoover, W. G. Canonical dynamics: Equilibrium phase-space distributions. *Phys. Rev. A* **1985**, *31*, 1695.
(88) Hockney, R., The potential calculation and some applications. *Methods Comput. Phys.* **1970**, *9*.
(89) Ryckaert, J.-P.; Ciccotti, G.; Berendsen, H. J. C. Numerical integration of the cartesian equations of motion of a system with constraints: molecular dynamics of *n*-alkanes. *J. Comput. Phys.* **1977**, *23*, 327.
(90) Senn, H. M.; Thiel, W. QM/MM Methods for Biomolecular Systems. *Angew. Chem., Int. Ed.* **2009**, *48*, 1198.
(91) Thorpe, I. F.; Brooks, C. L., III Conformational Substates Modulate Hydride Transfer in Dihydrofolate Reductase. *J. Am. Chem. Soc.* **2005**, *127*, 12997.
(92) Agarwal, P. K.; Billeter, S. R.; Rajagopalan, P. T.; Benkovic, S. J.; Hammes-Schiffer, S. Network of coupled promoting motions in enzyme catalysis. *Proc. Natl. Acad. Sci. U.S.A.* **2002**, *99*, 2794.
(93) Klinman, J. P. An integrated model for enzyme catalysis emerges from studies of hydrogen tunneling. *Chem. Phys. Lett.* **2009**, *471*, 179.
(94) Souaille, M.; Roux, B. Extension to the weighted histogram analysis method: combining umbrella sampling with free energy calculations. *Comput. Phys. Commun.* **2001**, *135*, 40.
(95) Rajamani, R.; Naidoo, K. J.; Gao, J. Implementation of an adaptive umbrella sampling method for the calculation of multidimensional potential of mean force of chemical reactions in solution. *J. Comput. Chem.* **2003**, *24*, 1775.
(96) IUPAC. Compendium of Chemical Terminology, 2nd ed. (the "Gold Book"). Compiled by McNaught, A. D.; Wilkinson, A.; Blackwell Scientific Publications: Oxford, U. K., 1997. XML on-line corrected version: http://goldbook.iupac.org (2006), created by M. Nic, J. Jirat, B. Kosata; updates compiled by A. Jenkins. ISBN 0-9678550-9-8. DOI: 10.1351/goldbook.M03931 (accessed May 14, 2012).
(97) Peters, B.; Heyden, A.; Bell, A. T.; Chakraborty, A. A growing string method for determining transition states: Comparison to the nudged elastic band and string methods. *J. Chem. Phys.* **2004**, *120*, 7877.
(98) Maragliano, L.; Fischer, A.; Vanden-Eijnden, E.; Ciccotti, G. String method in collective variables: Minimum free energy paths and isocommittor surfaces. *J. Chem. Phys.* **2006**, *125*, 024106.
(99) Miller, T. F.; Vanden-Eijnden, E.; Chandler, D. Solvent coarse-graining and the string method applied to the hydrophobic collapse of a hydrated chain. *Proc. Natl. Acad. Sci. U. S. A.* **2007**, *104*, 14559.
(100) Rare Events, Transition Pathways and Reaction Rates: Zero-Temperature String Method. http://www.math.princeton.edu/string/string0_implem.html (accessed May 14, 2012).
(101) Müller, K.; Brown, L. D. Location of saddle points and minimum energy paths by a constrained simplex optimization procedure. *Theor. Chim. Acta* **1979**, *53*, 75.
(102) Quapp, W.; Hirsch, M.; Heidrich, D. Bifurcation of reaction pathways: the set of valley ridge inflection points of a simple three-

dimensional potential energy surface. *Theor. Chem. Acc.* **1998**, *100*, 285.
(103) Chandler, D. Statistical mechanics of isomerization dynamics in liquids and the transition state approximation. *J. Chem. Phys.* **1978**, *68*, 2959.
(104) Montgomery, J. A.; Chandler, D.; Berne, B. J. Trajectory analysis of a kinetic theory for isomerization dynamics in condensed phases. *J. Chem. Phys.* **1979**, *70*, 4056.
(105) Rosenberg, R. O.; Berne, B. J.; Chandler, D. Isomerization dynamics in liquids by molecular dynamics. *Chem. Phys. Lett.* **1980**, *75*, 162.
(106) Hayoun, M.; Meyer, M.; Turq, P. Molecular Dynamics Study of a Solute-Transfer Reaction across a Liquid-Liquid Interface. *J. Phys. Chem.* **1994**, *98*, 6626.
(107) Nam, K.; Prat-Resina, X.; Garcia-Viloca, M.; Devi-Kesavan, L. S.; Gao, J. Dynamics of an Enzymatic Substitution Reaction in Haloalkane Dehalogenase. *J. Am. Chem. Soc.* **2004**, *126*, 1369.
(108) Nelson, K. V.; Benjamin, I. Effect of a Phase Transfer Catalyst on the Dynamics of an S_N2 Reaction. A Molecular Dynamics Study. *J. Phys. Chem. C* **2011**, *115*, 2290.
(109) Neria, E.; Karplus, M. A position dependent friction model for solution reactions in the high friction regime: Proton transfer in triosephosphate isomerase (TIM). *J. Chem. Phys.* **1996**, *105*, 10812.
(110) Neria, E.; Karplus, M. Molecular dynamics of an enzyme reaction: proton transfer in TIM. *Chem. Phys. Lett.* **1997**, *267*, 23.